Dynamic Behavior of Supercritical Extraction of Kerogen from Shale

A model is presented for the supercritical reaction-extraction of a solid component from a bed of porous particles through which the solvent flows. Accounted for are reaction at an intraparticle position, pore diffusion, interphase mass and heat transfer, and flow in a differential reactor. The behavior of the bed is dynamic since both temperature and concentration of extractable solid vary with time.

The model is compared with experimental data for the extraction with toluene of kerogen from a bed of Colorado shale particles. Curves of effluent bitumen concentration vs. time were measured and fitted with predicted curves to evaluate three parameters: preexponential factor and activation energy for the conversion of insoluble kerogen to soluble bitumen, and the diffusivity of toluene at the critical point. The predicted curves agreed well with the experimental results and gave reasonable values for the parameters. Rates of reaction-extraction as well as extraction curves exhibited a sharp dip as the reactor was heated through the critical temperature.

Jaime Triday, J. M. Smith
University of California
Davis, CA 95616

Introduction

Supercritical processes are receiving increasing attention for separating and recovering valuable products, particularly in the food and related industries. The very large increase in solubility when the solvent is raised to supercritical temperatures and pressures is one advantage. Others include enhanced mass transfer rates due to gaslike diffusivities and viscosities and recovery of fragile substances that would decompose in thermal processes.

While there is considerable information on the solubility and other equilibrium properties (Paulaitus et al., 1982) there is little information on rates of supercritical extraction. de Filippi et al. (1980) have proposed a model for the regeneration of spent activated carbon, but little else has been published about rates and process design for extracting substances from a solid phase.

Our objectives were twofold. The first was to develop a model applicable at supercritical conditions for reaction and extraction of solid particles in a fixed bed contacted with a flowing solvent. With minor modification, the model can be reduced to the simpler case where reaction does not occur, so that only the solubility is involved. Second, the model is applied to experimental data obtained for the extraction of kerogen from a Colorado oil shale, a process where reaction of insoluble kerogen to soluble bitumen occurs prior to extraction.

The proposed model accounts for two dynamic aspects. First, the change with time of the composition of extractant in the solid particle with the accompanying change in porosity. Second, the packed bed, initially at room temperature, is heated at a known rate to the specified supercritical temperature. This operating procedure corresponds to laboratory or pilot plant experiments in a fixed bed. A constant-temperature modification of the model could represent a moving bed of particles. The model contains three parameters: the activation energy and preexponential factor of the reaction, and the diffusivity of the extractant at the critical point.

The result of the experiments using oil shale is the curve of extract concentration vs. time. Data were obtained at supercritical and subcritical temperatures and pressures listed in Table 3. The model agrees well with the experimental data for reasonable values of the parameters and predicts the dip in the extraction curve as the reactor is heated through the critical temperature. This dip is due to the sharp decrease in density at the critical temperature, which introduces a significant convection contribution for intraparticle mass transport. The activation energy for converting kerogen to bitumen was 17 kJ/mol. This value is much less than pyrolysis activation energies, which are about 150 to 200 kJ/mol, (Braun and Burnham, 1986; Pan et al., 1985). In pyrolysis different reactions occur, producing different products including gases. Perhaps at supercritical condi-

tions the reaction is more similar to a solvation than to a thermal decomposition. The diffusivity at the critical point for bitumen was 7.7×10^{-9} m^2/s, a value that agreed with estimates from data for binary systems of pure hydrocarbons in toluene.

Experimental Method

On a laboratory scale, there are severe experimental problems in handling a moving bed of particles, or in instantaneously heating a fixed bed to supercritical temperatures. Therefore, a dynamic method was chosen in which a fixed bed of shale particles is contacted with the flowing solvent (toluene). The mass flow rate and pressure are held constant while the temperature is increased at a constant rate. After the desired final temperature is attained, the extraction is continued at constant temperature until the end of the run. To facilitate accurate calculations of extraction rates, a small bed (about 0.01 kg) of particles was used so that differential-reactor operation was approximated. A continuous measurement of the bitumen concentration was made after the reactor effluent stream had been reduced to 298 K and 101 kPa.

Apparatus

Figure 1 is a schematic view of the apparatus. The stainless steel reactor is a 0.45 m long tube, of 0.029 m ID and 4.8×10^{-3} m wall thickness. Stainless steel flanges seal the top and bottom of the reactor. Toluene from the feed tank (3) is pumped through a preheater coil wound around the reactor, and into the top of the reactor. The preheater-reactor assembly is placed in an electric furnace (1.4 kW maximum power) with a cylindrical cavity 0.33 m long and 6.0×10^{-2} m ID. The particles are supported in the central part of the reactor by a 100 mesh screen mounted on a hollow aluminum plug with a central hole 6.35×10^{-3} m in diameter and 0.18 m long, as shown in Figure 2.

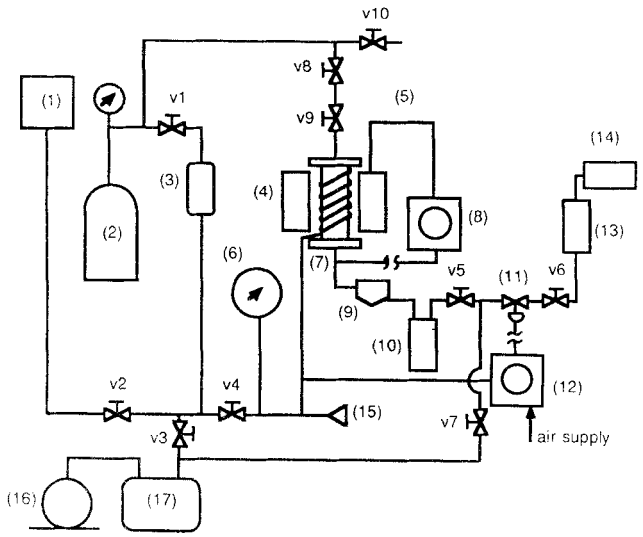

Figure 1. Experimental apparatus, including modifications for dispersion runs.

(1) Supply tank
(2) Nitrogen cylinder
(3) Feed tank
(4) Furnace
(5) Reactor
(6) Gauge
(7) Thermocouple
(8) Temperature Controller
(9) Filter
(10) Cooler
(11) Control valve
(12) Pressure controller
(13) Rotameter
(14) Spectrophotometer
(15) Rupture disk
(16) Mechanical vacuum pump
(17) Surge tank
v1–v10 Shut-off valves (v6, expansion valve)

A J-type thermocouple with the junction enclosed in a 1/16 in. (1.6 mm) stainless steel sheath is inserted up from the bottom of the reactor to measure temperature at the exit of the bed of particles. The specified error limits are 2.2 K between 273 and 550 K and 0.75% in the range 551 to 1,500 K. Pressure is measured with a Master test model gauge from Marsh Instrument Co. The temperature is controlled by an RKC proportional-integral controller and continuously recorded. The pressure is controlled with microneedle valve (11) which is activated with a Taylor Instrument Co. air controller (12).

Toluene flows downward in the bed of particles, through a Nupro 60 micron stainless steel filter (9), and cooler (10) where the temperature is reduced to 298 K. From there the pressure is reduced to near atmospheric by a control valve (11). Finally, the solution flows through a rotameter (13) and to the spectrophotometer (14). The latter instrument (Perkin Elmer Lambda 4B UV/VIS) combines the optical system with a microcomputer and is used on-line with a Fisher microflow cell to give a continuous recording of the transmittance (and adsorbance). The cell has a volume of 0.4×10^{-6} m^3 and path length of 0.01 m. Since the spectrophotometer could not be operated at supercritical conditions, the dispersion, residence time, and density change between reaction exit and spectrophotometer (i.e., through the cooler and expansion valve) had to be accounted for.

Shale properties and sample preparation

The oil shale, of Anvil Points Mine (Colorado), from Occidental Research Corp. provided the following ultimate analysis:

Carbon 17.3 wt. %
Hydrogen 1.82%
Nitrogen 0.69%
Sulfur 0.66%
Moisture 0.40%
Ash 67.3% (mineral carbonate content 22.3%)

Fischer assay gave 1.16×10^{-4} m^3 of oil per kg of shale, and the density was 2.15×10^3 kg/m^3. The kerogen and initial bitumen content was estimated to be 15.6 wt. % of the shale. The large

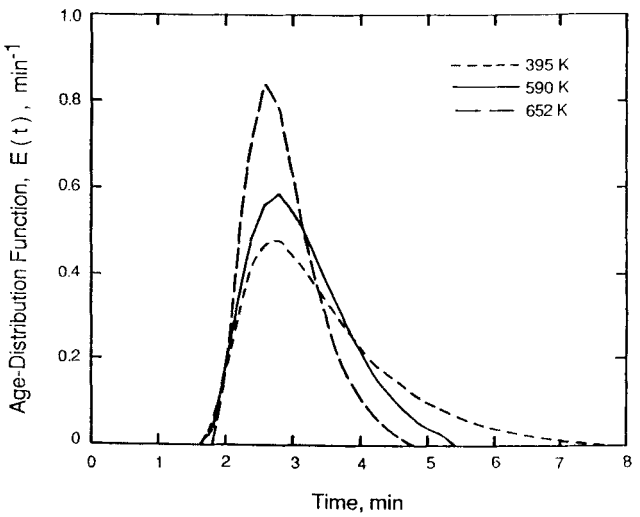

Figure 2. Effect of temperature on age distribution.
$P = 5.14$ MPa; $q = 1.20 \times 10^{-3}$ m^3/h

inorganic content consists primarily of carbonates, with some silicates and clays. The inorganics do not decompose at the maximum temperature (652 K) of our experiments. Hence, the only reaction considered was the conversion of kerogen to bitumen. The particles did not change shape during the supercritical runs.

The hydrocarbon material in shale is primarily kerogen, a high molecular weight organic material insoluble in most solvents. Trewhella et al. (1986) have reported from analysis of Green River (Colorado) shale that there are about four aliphatic chains present in 100 carbon atoms of kerogen and that the average hydrocarbon chain length per terminal methyl group is 6.5. The aromatic content indicated an average of three single rings (benzenelike) or two fused rings (naphthalenelike) per 100 carbon atoms. Shale initially contains some soluble hydrocarbon material (bitumen), usually about 10% of the total organic content. Our research was concerned with the conversion and extraction of kerogen. Hence, the bitumen present initially was removed prior to introducing samples into the apparatus.

Samples of shale were prepared by first grinding and sieving. Fractions between Tyler screens 7 and 8 (average size 2.6×10^{-3} m) and between openings 0.185 and 0.313 in. (average size 6.4×10^{-3} m) were retained. The particles were then fluidized in air to remove dust and heated at 350 K for 24 h to remove moisture. Following the procedure developed by Yucelen et al. (1986) to remove initial bitumen, weighed samples were treated with toluene at ambient conditions for 15 days. Then the samples were filtered, washed, and dried at 350 K for 24 h. It may be that some bound water was not removed by this pretreatment. The effect of possible removal of bound water was probably small and was not considered. A final weighing showed that for the 2.6×10^{-3} m particles 9.4 wt. % of the original organic material had been removed, meaning that the treated samples had a kerogen content of 13.6 wt. % of the shale. For the 6.4×10^{-3} m particles, the initial bitumen removed was 8.0%, so that the kerogen content of the treated samples was 14.0%. The treated samples were kept in a dessicator and used as needed for the extraction runs. After a run the particles were again dried and weighed.

Toluene was chosen as the solvent since the extracted material, bitumen, remained in solution at the room temperature and pressure of the spectrophotometer. Analytical grade toluene was used and purified after each run by distillation in a high-efficiency packed column. Comparison of the spectra of distilled and initial toluene in the visible range failed to show impurities in the distilled solvent.

Operating procedure

About 0.01 kg of oil-shale particles at room conditions are placed in the reactor and the system is evacuated. After toluene flow is started, the pressure is adjusted from the nitrogen cylinder, and the pressure controller set. Next, the flow rate is fixed, the furnace turned on, and the spectrophotometer program started. This marks the start of a run. The temperature gradually increases to the desired final temperature, after which it is controlled at the final value. The end of the run (usually at 150 min) is when toluene is exhausted in the feed tank.

Effluent bitumen concentration

The absorbance of the solution is continuously measured at 298 K and 101 kPa in the spectrophotometer. Preliminary experiments showed that the absorption spectra of the solution did not change with time during a run. This indicates that the chemical species and their concentration in the extracted bitumen are constant during a run and means that the absorbance A is a measure of the concentration of bitumen in the toluene solution. The absorbance was measured at 440 nm since at this wavelength the absorbance was high and the relation between concentration and absorbance was linear. The linearity was verified by measurements with successively diluted solutions. Then Beer's law is applicable:

$$A(t) = aC_b(t) \tag{1}$$

where a is the absorptivity constant at 440 nm.

The known loss in mass ∂_m of the particles for the whole run of time t_t is related to the bitumen concentration $C_{b,a}$ by the mass balance:

$$\partial_m = \int_0^{t_t} qC_{b,a}(t)\, dt \tag{2}$$

Multiplying Eq. 1 by the flow rate q and integrating from 0 to t_t gives for the absorptivity constant

$$a = \frac{1}{\partial_m} \int_0^{t_t} qA(t)\, dt \tag{3}$$

Using Eq. 3 for a in Eq. 1 gives the expression for the concentration:

$$C_{b,a}(t) = \frac{\partial_m A(t)}{\int_0^{t_t} qA(t)\, dt} \tag{4}$$

as a function of the measured absorbance.

Dispersion and density correction

The measured $C_{b,a}$ vs. t curve needs to be corrected for dispersion and density changes between the reactor exit and the spectrophotometer. The dispersion effect was measured by injecting a pulse of concentrated bitumen solution at the exit of the reactor and measuring the absorbance at the spectrophotometer. The injection system shown in Figure 1 consists of two shut-off valves connected to a capillary tube, which ends at the reactor exit. The age-distribution function is given in terms of the measured absorbance by the expression

$$E(t) = \frac{A(t)}{\int_0^{\infty} A(t)\, dt} \tag{5}$$

Table 1 gives the experimental conditions for the dispersion runs. The effects of temperature and pressure were measured at constant flow rate ($q = 1.2 \times 10^{-3}$ m^3/h at 298 K and 0.1 MPa) over the same ranges as covered in the extraction runs. Figure 2 shows the effect of temperature on the age distribution at 5.14 MPa pressure. Dispersion decreases as the temperature increases. The effect of pressure was measured both at temperatures near the critical (517–532 K) and in the supercritical range (650 K). In both temperature ranges the pressure effect on $E(t)$ was less than experimental uncertainties. Hence, the

Table 1. Dispersion Run Conditions

RTD Run No.	T K	T_r	P MPa	P_r
1	338	0.57	5.14	1.25
2	395	0.67	5.14	1.25
3	458	0.77	5.14	1.25
4	517	0.87	5.14	1.25
5	590	1.00	5.14	1.25
6	652	1.10	5.14	1.25
7	652	1.10	5.14	1.25
8	536	0.91	3.69	0.90
9	650	1.10	5.55	1.35
10	532	0.90	5.55	1.35

Flow rate, $q = 1.20 \times 10^{-3}$ m^3/h at 298 K, 0.10 MPa

dispersion correction was made for the effect of temperature but not for pressure. The density correction is discussed later.

Reaction-Extraction Model

It is supposed that the extractable material is uniformly distributed throughout the porous particles. In shale the initial porosity is caused by the removal of the soluble bitumen initially present. The particles are assumed to be spherical and to retain their shape during reaction and extraction, although the porosity increases.

The observed large influence of temperature level indicates that the chemical reaction of kerogen to bitumen significantly affects the overall process. Also, a model based solely upon solubility did not agree with the data. The nature of the reaction that occurs at supercritical conditions is not clear. One possibility is a two-step sequence: a slow reaction followed by a fast, solution step:

$$\text{Kerogen (s)} \rightarrow \text{Bitumen (s)} \tag{6}$$

$$\text{Bitumen (s)} + \text{Toluene (l)} \rightarrow \text{Bitumen (solution)} \tag{7}$$

The work of Yucelen et al. (1986) showed that kerogen slowly decomposed in a nitrogen atmosphere at subpyrolysis but supercritical temperatures (611 K) to a product soluble in toluene (bitumen). About 26% of the original kerogen was decomposed in 5 h. This provides evidence for the first step in the above sequence. However, in our supercritical experiments with toluene at the same temperature about 60% of the kerogen was extracted in 2.5 h. This suggests that the conversion occurs at least partially by a single-step, activated solvation process:

$$\text{Kerogen (s)} + \text{Toluene (l)} \rightarrow \text{Bitumen (solution)} \tag{8}$$

In both cases the rate of extraction can be described by the same expression since the concentration of toluene is large and nearly constant.

We have assumed that removal of the extractable solid is first order and irreversible. Applied to shale this means that the mass rate of disappearance of kerogen, or production of bitumen, can be described by

$$\frac{dC_k}{dt} = -k_o\left[\exp\left(-\frac{E_a}{R_gT}\right)\right]C_k \tag{9}$$

where C_k is the mass of kerogen per unit volume of particle and $C_k = C_{k_o}$ at $t = 0$. A first-order decomposition for pyrolysis of kerogen has been found to be applicable in several investigations (Braun and Burnham, 1986; Charlesworth, 1985; Wallman et al., 1981; Yang and Sohn, 1985, Richardson et al., 1982; Yucelen et al., 1986; Pan et al., 1985. Products of pyrolysis include bitumen, gas, and coke. In supercritical extraction no gas or coke was observed. The increase in porosity is related to the rate of disappearance of extractable solid:

$$\frac{d\epsilon_p}{dt} = -\frac{1}{\rho_k}\frac{dC_k}{dt} \tag{10}$$

The mass balance of bitumen within the particle may be written

$$\frac{\partial(\epsilon_pC_b)}{\partial t} = \frac{1}{r^2}\frac{\partial}{\partial r}\left[r^2\left(D_e\frac{\partial C_b}{\partial r} - C_bv_r\right)\right] + k_oC_k\exp\left(-\frac{E_a}{R_gT}\right) \tag{11}$$

The convective term involving the radial velocity v_r in the pores is necessary because of the large change in fluid density during the heating period, particularly when the temperature is near the critical value (592 K). In Eq. 11 the extent to which the solution process occurs, Eq. 8, requires the assumption that all the kerogen present is exposed to toluene throughout the run.

The convective velocity can be ascertained from the overall continuity equation:

$$\frac{\partial(\epsilon_p\rho)}{\partial t} + \frac{1}{r^2}\frac{\partial}{\partial r}[r^2(\rho v_r)] = 0 \tag{12}$$

Integrating Eq. 12 with respect to radial position from $r = 0$ to r gives

$$v_r = -\frac{r}{3\rho}\frac{d}{dt}(\epsilon_p\rho) \tag{13}$$

The initial and boundary conditions for Eq. 11 are

$$t = 0, \quad C_b = 0 \quad \text{for all } r \tag{14}$$

$$t > 0, \frac{\partial C_b}{\partial r} = 0 \quad \text{at } r = 0 \tag{15}$$

$$-D_e\frac{\partial C_b}{\partial r} + C_bv_r = k_c[(C_b)_{r=R_o} - C_{b,b}] \tag{16}$$

The tortuosity factor must be known before the effective diffusivity in Eq. 11 can be evaluated. The relatively large macropores in shale suggest a lower tortuosity factor than for catalyst particles. Therefore, the formulation of Chang (1982), which expresses the tortuosity factor as $2 - \epsilon_p$, was used. Then

$$D_e = D\frac{\epsilon_p}{2 - \epsilon_p} \tag{17}$$

The intraparticle temperature T is a function of radial position in the particle, bed depth, and time. During the heating period the bulk solution temperature increases and the particle temperature rises by transfer of energy from the solution. As an

estimate, the intraparticle gradient during the heating period can be found by solving the unsteady heat conduction equation for a spherical particle in the absence of reaction. For an initially uniform temperature profile and a surface temperature increasing at a rate of m, K/s, the difference ΔT between the surface and center temperature is given by

$$\Delta T = \frac{mR_o}{6\eta_{os}} \tag{17}$$

where η_{os} is the thermal diffusivity of shale (about 4.3×10^{-7} m^2/s for raw shale). For the largest particles, ΔT is but 0.3 K for a heating rate m of 0.14 K/s, which corresponds to our experimental value. The heat of conversion of kerogen to bitumen cannot be greater than the activation energy for this endothermic process. As shown later, E_a is only about 17 kJ/mol. For this value of intraparticle ΔT would not be significantly increased by considering the heat of reaction. Hence, the particles will be assumed to have a uniform temperature. Then, the energy balance for the particles may be written

$$\frac{dT}{dt} = \frac{ha_m}{\rho_{os} C_{p_{os}}} (T_b - T) \tag{18}$$

with initial condition

$$t = 0, \quad T = T_b = 298 \text{ K} \tag{19}$$

With appropriate values of the quantities in Eq. 18 for our experiments, the temperature difference $T_b - T$ is in the range 0 to 1.5 K. This difference was accounted for in applying the model, but the effect is probably within experimental uncertainties.

Equations 9–11 and 18 describe the behavior of a single particle during extraction and reaction. The next requirement is to relate the local $C_{b,b}$ to the concentration leaving the bed.

Since a small bed was used, differential reaction behavior was approached, meaning that the rate of extraction was the same for all particles. Under these conditions axial and radial dispersion are negligible. As shown by Ludwig et al. (1985), the arithmetic average $\bar{C}_{b,b}$ of the entrance and exit bitumen concentrations in the toluene may be used to evaluate the rate of reaction for the whole bed, even though the process is dynamic. Then

$$\bar{C}_{b,b} = \frac{C_{b,e} + 0}{2} \tag{20}$$

and

$$\frac{\partial C_{b,b}}{\partial x} = \frac{C_{b,e} - 0}{L} = \frac{2\bar{C}_{b,b}}{L} \tag{21}$$

The mass balance in the reactor is

$$\epsilon_b \frac{\partial C_{b,b}}{dt} + u \frac{\partial C_{b,b}}{\partial x} = k_c a_m (1 - \epsilon_b)[(C_b)_{r=R_o} - C_{b,b})] \tag{22}$$

With Eqs. 20 and 21, Eq. 22 can be expressed in terms of the average concentration as

$$\frac{d\bar{C}_{b,b}}{dt} + \frac{2u}{\epsilon_b L} \bar{C}_{b,b} = \frac{3k_c}{R_o} \frac{1 - \epsilon_b}{\epsilon_b} [(C_b)_{r=R_o} - \bar{C}_{b,b}] \tag{23}$$

where a_m for a spherical particle is $3/R_o$ and at $t = 0$, $\bar{C}_{b,b} = 0$. Equation 23 combined with Eq. 20 provides a relation between the bitumen concentration $C_{b,e}$ at the exit of the reactor, and the concentration $(C_b)_{r=R_o}$ at the particle surface. The bulk fluid temperature T_b is uniform throughout the bed according to the differential-reactor approximation.

Coupled Eqs. 11 and 23, along with the boundary and initial conditions and auxiliary equations, may be solved for $C_{b,e}$ as a function of time. These predicted extraction curves can then be compared with the measured curves to evaluate the model. The method was first to make the equations dimensionless and then use a fully implicit, finite-difference solution procedure (Triday, 1987). The measured temperature profile provides the bulk fluid temperature needed for the solution. Mathematical details and solution stability questions are discussed by Triday.

After $C_{b,e}$ was calculated, the rate of extraction Ω per unit initial mass m_o of shale was obtained from a mass balance of bitumen around the differential reactor:

$$m_o \Omega = 2q\bar{C}_{b,b} + \epsilon_p V \left(\frac{d\bar{C}_{b,b}}{dt}\right) \tag{24}$$

where q is the flow rate at reactor temperature and pressure and V the reactor volume.

To obtain a numerical solution the physical and transport properties must be known and the effects of dispersion and density changes between the reactor exit and the spectrophotometer accounted for.

Physical and Transport Properties

Solution properties

The density of the solvent has a strong influence in supercritical extraction since it affects the viscosity, and therefore the diffusivity, as well as mass and heat transfer coefficients. Since toluene densities in the supercritical region were not available, the generalized correlation of Lee and Kesler (1975), based upon a three-parameter equation of state, was used. It has proven suitable for calculations in the critical and compressed, subcooled regions. The viscosity of toluene at high pressures was calculated by the residual viscosity correlation of Stiel and Thodos (1964b). This requires the low-pressure gas viscosity, which was estimated by the Golubev (1959) method. Results for the density and viscosity at 5.14 MPa are shown in Figure 3.

The heat capacity of toluene in the ideal-gas state was

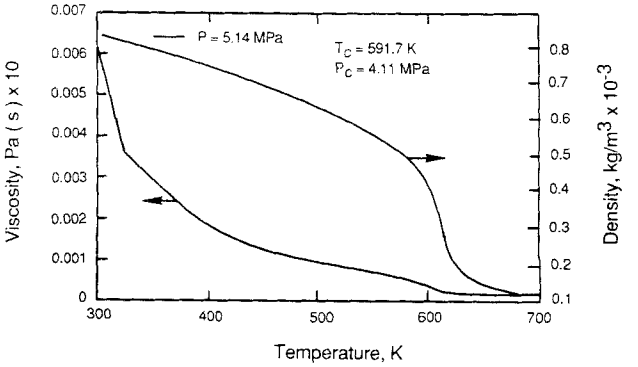

Figure 3. Density and viscosity of toluene.
$P = 5.14$ MPa

obtained from the data bank given by Reid et al. (1977). Then C_p at supercritical conditions was calculated using the Lee-Kesler equation of state. The thermal conductivity at low pressure was determined from the correlation of Roy and Thodos (1970) and corrected for the effect of pressure with the Stiel and Thodos (1964a) residual correlation. Complete results for C_p, λ, μ, and ρ for toluene in the supercritical region are given by Triday (1987). Since the solutions were dilute the properties of toluene were used for all solution properties.

Also needed is the diffusivity of bitumen in toluene. Experimental data in the supercritical region are meager. However, Sun and Chen (1985a,b, 1986) have measured molecular diffusivities for benzene, toluene, *p*-xylene, naphthalene, phenanthrene, and other components in either cyclohexane, *n*-hexane, or ethanol solvents. Their correlation agreed with the data within 4%. Bitumen is not well characterized chemically but consists of numerous hydrocarbon-type substances. We have used the Sun and Chen correlation only for the effect of pressure and temperature. Taking as a reference the diffusivity of bitumen in toluene at the critical point D_c, the correlation may be written

$$D = D_c T_r/(\mu/\mu_c)^{0.796} \tag{25}$$

where D, T_r, and μ refer to values at the chosen supercritical condition.

Since the composition of bitumen is unknown, we took D_c as an adjustable parameter in evaluating the model (see Results section). However, an estimate can be made for D_c from the Sun and Chen correlation. Considering the substances listed in Table 2 as components of bitumen, the diffusivities so calculated are given in the last column. The values do not differ greatly and have an average of 5.3×10^{-9} m^2/s. The variation in D with temperature as calculated from Eq. 25 at $P = 5.14$ MPa is shown in Figure 4. The critical diffusivity of 7.7×10^{-9} m^2/s is that found by comparing predicted and measured extraction curves, as described later.

No data were found for mass and heat transfer coefficients in the supercritical region between fluid and particles in packed beds. The correlations of Wakao and Kaguei (1982) were employed for calculating k_c and h:

$$\frac{k_c d_p}{D} = 2.0 + 1.10(Sc)^{1/3}(Re)^{0.6} \tag{26}$$

$$\frac{k d_p}{\lambda} = 2.0 + 1.10(Pr)^{1/3}(Re)^{0.6} \tag{27}$$

Table 2. Diffusivities in Toluene at the Critical Point

Solute	Crit. Vol. m^3/kmol	Diffus. $D_c \times 10^9$ m^2/s
n-Hexane	0.370	5.32
n-Hepatane	0.432	4.92
Benzene	0.259	6.36
Naphthalene	0.410	5.05
Tetralin	0.425	4.96

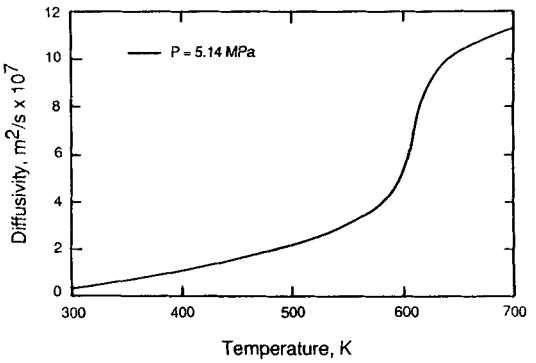

Figure 4. Diffusivity of bitumen in toluene.
P = 5.14 MPa

Shale properties

The porosity of the shale at the start of a run (after dissolving the bitumen initially present) was 0.036. The value of ϵ_p at the end of a run varied with the operating conditions; for example, for run 2, Table 3, the final value was 0.264.

The density, 2.15×10^3 kg/m^3, was taken to be independent of temperature. No information was found for temperature effects. The heat capacity of the raw shale was calculated from the correlation of McCarthy et al. (1976):

$$C_{p_{sr}} = 0.720 + (2.80 \times 10^{-4} + 1.63F)T \tag{28}$$

where F is the Fischer assay, m^3 oil/kg. Correlations for spent (by pyrolysis) shale are also available, but the raw shale result is believed to represent better the properties at supercritical extraction conditions. Thermal properties are relatively unimportant since temperature variations in the reactor between fluid and particle, and within the particle, are very small.

To estimate intraparticle temperatures requires the thermal diffusivity of shale. This was estimated to be 4.3×10^{-7} m^2/s for our shale from the raw-shale correlation of McCarthy et al.

Density and Dispersion Corrections

The concentration of bitumen was measured at the spectrophotometer at 298 K and 0.1 MPa, while the model predicts the concentration at reactor exit conditions. To evaluate the model the predicted value at the reactor exit was corrected to apply at 298 K and 0.1 MPa. The correction required accounting for the change in density and the dispersion between reactor exit and the spectrophotometer.

The concentration at 298 K and 0.1 MPa, corrected for the density effect, is given by

$$C_{ba} = \frac{\rho_a}{\rho_e} C_{b,e} \tag{29}$$

This correction can be large, as seen from the potentially large density change in Figure 3.

The dispersion effect was measured experimentally, resulting in the age distribution shown in Figure 2. Using the known age distribution, the concentration at the spectrophotometer is re-

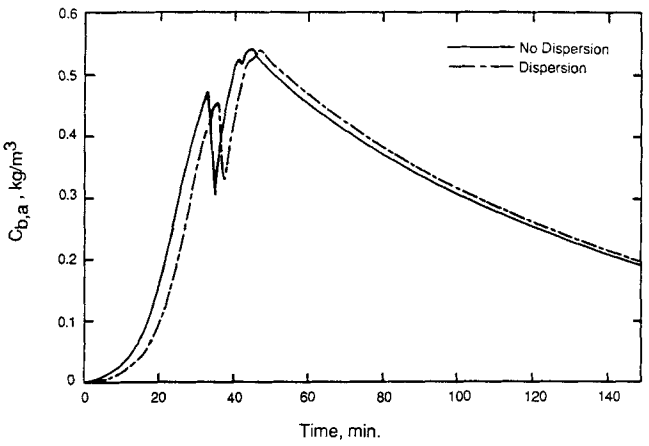

Figure 5. Effect of dispersion on bitumen concentration.
T = 298 K; P = 0.1 MPa (age distribution function at 652 K, 5.14 MPa)
Conditions of run 2

lated to $C_{b,e}$ by the equation

$$C_{b,a} = \rho_a \int_0^t \frac{C_{b,e}}{\rho_e} E(t - t')\, dt' \qquad (30)$$

Figure 5, for a final temperature of 652 K and at 5.14 MPa—the conditions of extraction run 2, Table 3—shows predicted extraction curves with and without the dispersion correlation. The effect is not very large and is most pronounced during the initial period of a run. Both curves in Figure 5 have been corrected for the density change and exhibit an interesting dip as the temperature passes through the critical value.

Results

Experimental runs

Table 3 lists conditions for typical runs of four kinds: supercritical (runs, 2, 5, 6, 8, 14), subcritical (runs 3, 4, 7), two-phase (run 16), and pyrolysis (runs 1, 11). Figure 6 is a generalized diagram of reduced density on which the path of run 2 is marked. Each run follows a horizontal line from 298 K (T_r =

Table 3. Extraction Run Conditions*

Extrac. Run No.	P MPa	P_r	T K	T_r	$m_o \times 10^3$ kg	Yield %	$q \times 10^3$ m^3/h
1	5.14	1.25	672	1.13	10.301	116	1.20
2	5.14	1.25	654	1.11	10.228	67	1.22
3	5.14	1.25	528	0.89	10.014	12	1.22
4	5.14	1.25	476	0.80	10.052	5.4	1.19
6	5.95	1.45	652	1.10	10.239	70	1.21
7	3.69	0.90	533	0.90	9.638	9.9	1.21
14	5.14	1.25	648	1.09	10.075	63	1.18
16	3.69	0.90	650	1.10	10.092	59	1.19
8	5.14	1.25	647	1.09	10.912	62	1.21
11	5.14	1.25	667	1.13	11.786	121	1.21

	*Run Nos.	
	1–4, 6, 7, 14, 16	8, 11
d_p	2.6 × 10^{-3} m	6.4 × 10^{-3} m
Kerogen in shale at start of run (after removal of bitumen initially present)	13.6 wt. %	14.0 wt. %

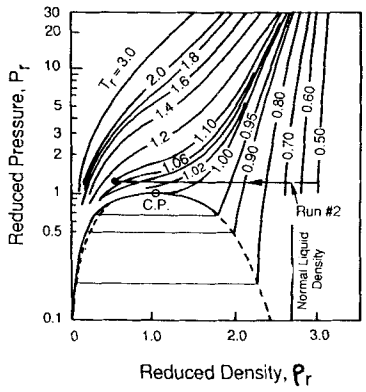

Figure 6. Reduced density as a function of reduced pressure and reduced temperature, generalized diagram.

0.50) during the heating period and continues at the end point of the line until the end of the run. Runs 1 and 11 are at high enough temperatures for pyrolysis to occur. For these cases some particles were cracked and broken and also char was formed. In run 7 the pressure was below the critical value but the end temperature was also less than the critical. Hence the toluene was subcritical but was in the single-phase (liquid) region. In run 16 the fluid passed through the two-phase region during the heating period.

Tables 3 and 4 also give the yield for the entire run, defined as the percent of the original kerogen extracted. Yields for the supercritical runs are much greater than those for subcritical runs 3, 4, and 7, showing the advantage of supercritical operation. The yields at pyrolysis conditions, runs 1 and 11 were greater than 100%.

For runs near the critical pressure, oscillations in both temperature and pressure were observed as the temperature approached the critical value. This was due to the sensitivity of density to temperature, Figure 3. Figure 7 shows the oscillations measured for a run at the critical pressure.

The model was developed for supercritical conditions, so most of the runs were made at $P_r > 1.0$ and $T_r > 1.0$. It is not expected that the model would be applicable for runs at pyrolysis or oscillating conditions. Run 2 is considered typical, P_r = 1.25 and at the final temperature T_r = 1.11. Figure 8 shows results for two runs at conditions approximating those of run 2. It was not possible to reproduce exactly the temperature profile, as indicated in the figure. Taking into account the differences in temperature,

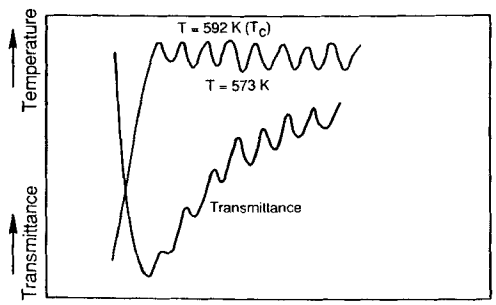

Figure 7. Absorption curve in critical region.
Temperature at reactor
Conditions: d_p = 2.6 × 10^{-3} m; P = 4.11 MPa (P_c); q = 1.20 × 10^{-3} m^3/h

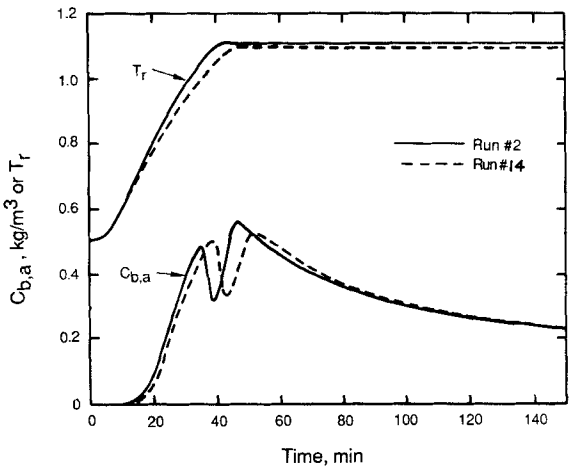

Figure 8. Experimental extraction curves, reproducibility test.

$d_p = 2.6 \times 10^{-3}$ m; $P = 5.14$ MPa ($P_r = 1.25$)

	Run #2	Run #14
Final T	654 K	648 K
	($T_r = 1.11$)	($T_r = 1.09$)
$q \times 10^{-3}$ m^3/h	1.22	1.18

the concentration curves show good reproducibility. The beginning of the dip in the concentration curves occurs at about the critical temperature for both runs.

Figure 9 shows the large effect of temperature. The curves are all for $P_r = 1.25$ and so are in the single-phase region. The large temperature effect suggests an activated process for converting kerogen to bitumen.

Figure 10 displays the effect of pressure at $T_r = 1.1$. Pressure has an effect on the concentration only when the temperature is in the critical region. Although the temperature profiles are somewhat different, the dip in the concentration curves is less at the higher pressure. That the dip is due to the temperature going through the critical value is confirmed in Figure 11, where the results for run 3 ($P_r = 1.25$) and run 7 ($P_r = 0.90$) are shown.

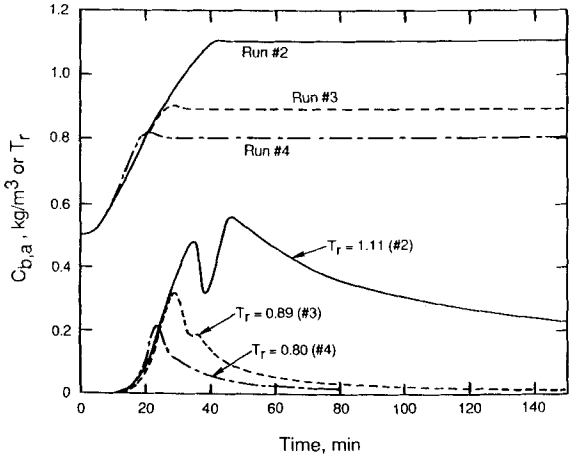

Figure 9. Effect of temperature on experimental extraction curves.

$d_p = 2.6 \times 10^{-3}$ m; $P = 5.14$ MPa ($P_r = 1.25$)

	Run #2	Run #3	Run #4
Final T	654 K	529 K	476 K
	($T_r = 1.11$)	($T_r = 0.89$)	($T_r = 0.80$)
$q \times 10^{-3}$ m^3/h	1.22	1.22	1.20

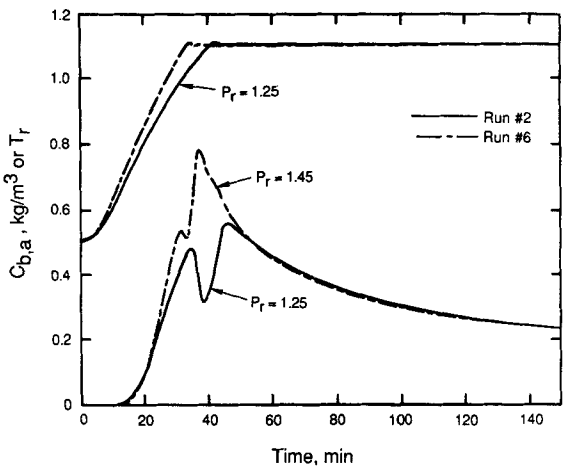

Figure 10. Effect of pressure on experimental extraction curves.

$d_p = 2.6 \times 10^{-3}$ m^3/h

	Run #2	Run #6
P, MPa	5.14	5.95
	($P_r = 1.25$)	($P_r = 1.45$)
Final T	654 K	652 K
	($T_r = 1.11$)	($T_r = 1.10$)
$q \times 10^{-3}$ m^3/h	1.22	1.21

The temperature did not reach the critical in either of these runs. The dip has nearly disappeared. Also, the effect of pressure is negligible. The difference between the two concentration curves is due to the slightly different temperature profiles.

The particle size was changed by a factor of 2.5, corresponding to a sixfold difference in intraparticle diffusion resistance. Experimental extraction curves for these two sizes at $P_r = 1.25$ and T_r = about 1.1 were approximately the same. The curve for the larger size was slightly delayed indicating some diffusion resistance. However this effect is small with respect to that of temperature.

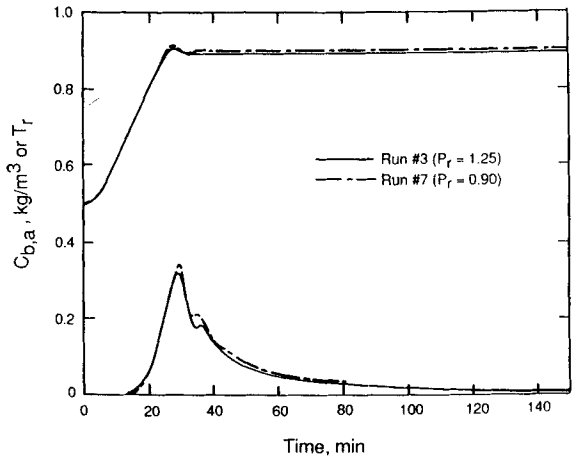

Figure 11. Effect of pressure on experimental extraction curves at $T_r < 1$.

$d_p = 2.6 \times 10^{-3}$ m

	Run #3	Run #7
P, MPa	5.14	3.69
	($P_r = 1.25$)	($P_r = 0.90$)
Final T	529 K	533 K
	($T_r = 0.89$)	($T_r = 0.90$)
$q \times 10^{-3}$ m^3/h	1.22	1.21

Table 4. Optimum Parameter Values from the Fit of Data

Extrac. Run No.	E_a, kJ/mol	$k_o \times 10^3$ s^{-1}	$D_c \times 10^9$ m^2/s	RMS Dev.
2	16.1	3.10	7.32	0.024
14	16.1	2.99	7.68	0.026
3	17.2	3.52	7.51	0.031
4	17.2	3.62	6.99	0.030
6	17.6	4.68	9.48	0.036
7	16.7	3.33	7.12	0.044
8	18.1	4.14	8.10	0.032

Model predictions

The three adjustable parameters are activation energy E_a, preexponential factor k_o, and diffusivity of bitumen in toluene at the critical point D_c. For comparison with the experimental values, the concentrations $C_{b,e}$ from the model were corrected for density changes and dispersion between reactor exit and spectrophotometer, as already described. Then the model parameters were evaluated by minimizing the objective function

$$\Phi(E_a, k_o, D_c) = \sum_{i=1}^{N} [(C_{b,a})_{\text{exp}} - (C_{b,a})_{\text{pred}}]^2 \qquad (31)$$

where $C_{b,a}$ refers to the bitumen concentration at the spectrophotometer. Analytical derivatives were not available for Φ with respect to E, k_o, and D_c, so they were evaluated numerically using finite differences. The multivariable secant method (Triday, 1987) was employed for solving the three sets of equations.

Table 4 gives optimal parameter values for the runs in the super- and subcritical regions. The last column in Table 4 shows the goodness of fit as determined by the root mean square deviation

$$rmsd = \left(\frac{\Phi}{N}\right)^{1/2} \qquad (32)$$

The parameter values agree reasonably well for runs at different temperatures and pressures and for the two particle sizes.

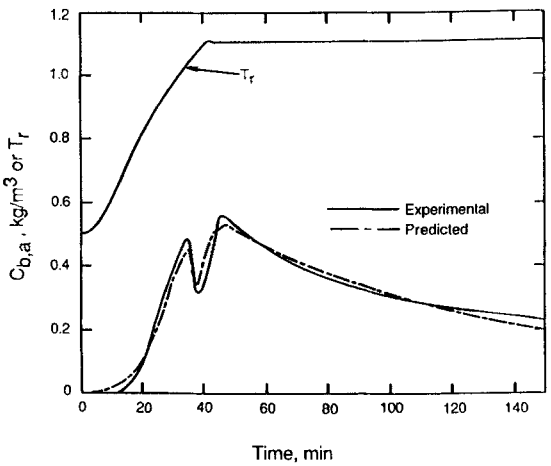

Figure 12. Predicted and experimental extraction curves for run 2.
$T_r = 1.11$; $P_r = 1.25$; $d_p = 2.6 \times 10^{-3}$ m

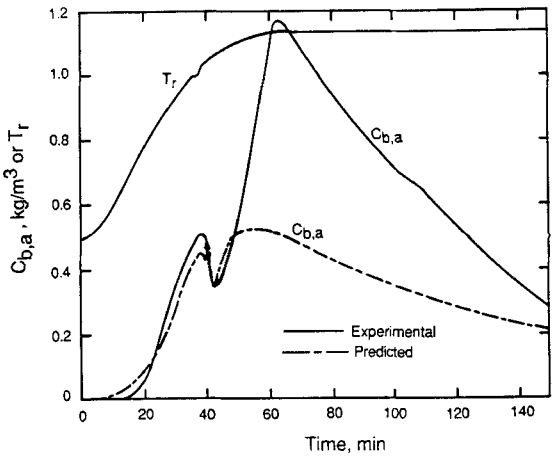

Figure 13. Predicted and experimental extraction curves for pyrolysis conditions, run 1.
$T_r = 1.13$; $P_r = 1.25$; $d_p = 2.6 \times 10^{-3}$ m

Figure 12 displays predicted and experimental curves of $C_{b,a}$ for the supercritical conditions of run 2. The agreement lends confidence to the model. In addition, the model predicts well the dip in the curves near the critical temperature, indicating that the changes in density and dispersion are accounted for adequately. Similar agreement was found for runs 6–8 at other temperatures, pressures, and particle size.

Figure 13 shows experimental and predicted (using parameter values for run 2) concentration curves for run 1 where pyrolysis occurred. It is clear that the model parameters (particularly k_o and E_a) must be different for the pyrolysis process.

Discussion

Parameter values

A first-order rate equation, Eq. 9, was used for the conversion of kerogen to bitumen by analogy to rate equations that represent pyrolysis data. The activation energy, about 17 kJ/mol, is much less than the 150–200 kJ/mol found for the thermal process of pyrolysis. The products are no doubt different for the two processes, with those from supercritical extraction being less degraded. In addition, the low value suggests that the supercritical toluene somehow aids the conversion. To describe better the potential influence of toluene, chemical analysis of bitumen is needed. The rates of reaction are also different. Pan et al. (1985) reported at 673 K a rate constant, $k_o \exp(-E_a/R_gT)$, of 5.54×10^{-4} s^{-1}, while extrapolating the results for run 2, Table 4, gives 1.74×10^{-4} s^{-1}.

The average of the values in Table 4 for D_c is 7.7×10^{-9} m^2/s. This is similar to but somewhat higher than the estimated values from the Sun and Chen correlation (1986) shown in Table 2. In view of the unknown composition of bitumen, 7.7×10^{-9} m^2/s appears to be a reasonable value. In the optimization procedure the effect of D_c on Φ was less than the effects of k_o and E_a. Typical values for diffusivities of hydrocarbons in liquids at atmospheric pressure are around 10^{-9} m^2/s or seven times less than D_c at supercritical conditions found from the analysis of our data.

Dip in the extraction curves

Both predicted and experimental extraction curves at the spectrophotometer show a dip when the temperature rises

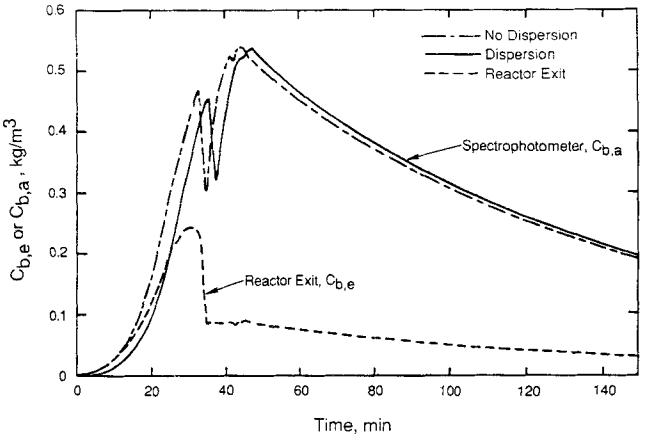

Figure 14. Predicted extraction curves for run 2.
--- At reactor exit, $T_r = 1.25$; $P_r = 1.11$
At spectrophotometer, $T = 298$ K; $P = 0.1$ MPa
—·— Neglecting dispersion —— With dispersion correction

through the critical value, Figures 13–17. Hence, model predictions may be used to explain the drop in concentration. The magnitude of the decrease at the spectrophotometer is greatest near the critical pressure.

The dashed curve in Figure 14 shows the predicted extraction curves at reactor exit conditions ($P_r = 1.25$, $T_r = 1.11$) using parameter values for run 2, Table 4. During the early part of the run the concentration at the reactor exit increases due to the increasing temperature and resulting increase in rate of conversion of kerogen to bitumen. As the critical temperature is approached the convection term becomes more important due to the sharp decrease in density, as shown in Figure 3. Also, intraparticle diffusion is increased because of the increase in diffusivity. At subcritical temperatures the bitumen accumulates in the porous particles, due to low convection and diffusion. When the critical temperature is reached this high-concentration bitumen is rapidly expelled from the pores due primarily to convection. This causes a subsequent sharp drop in the concentration in the bulk solution as bitumen builds up in the solution in the pores. The concentration continues to fall slowly during the final stage

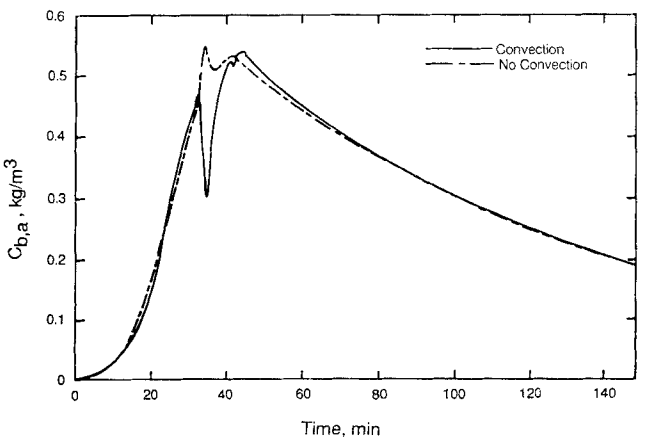

Figure 15. Effect of intraparticle convection on predicted extraction curve at spectrophotometer.
Conditions of run 2, $T = 1.11$; $P_r = 1.25$
No dispersion correction

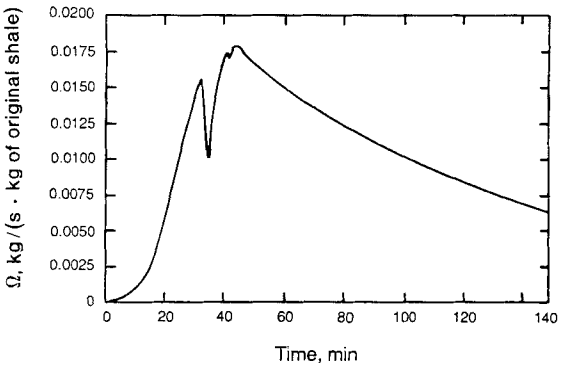

Figure 16. Predicted rate of extraction for run 2.
$T_r = 1.11$; $P_r = 1.25$; $q = 1.22 \times 10^{-3}$ m^3/h

of the run at the reactor exit. Predicted intraparticle profiles of density, diffusivity, and concentration provided a more detailed explanation for the dip (Triday, 1987).

Also displayed in Figure 14 are predicted concentrations at spectrophotometer conditions ($T = 298$ K, $P = 0.1$ MPa), one curve neglecting dispersion and the other including this effect. Both curves include the convection effect and the density correction according to Eq. 29, and both are at the same temperature and pressure through the run. They show that after the drop, the concentration first increases because of the higher temperature and then falls as the kerogen is removed (decrease in C_k). As in Figure 5, the curves are not greatly affected by dispersion; density is the dominant effect.

The importance of the convection term is shown in Figure 15 where predicted concentration curves at $T = 298$ K and $P = 0.1$ MPa are shown for the same conditions as in Figure 16. The solid curve reproduces that with dispersion in Figure 14, while the dashed curve neglects convection. The severe drop in concentration at the critical temperature is not predicted if convection is neglected. Note that the experimental curve for run 2, Figure 12, also shows the sharp drop.

Rate of extraction

Figure 16 illustrates rates of extraction calculated by Eq. 24 using the predicted extraction curve for run 2, Figure 13. The exit concentration at reactor conditions is twice the average concentration according to the differential reactor approximation, Eq. 20. Similar rate curves could be calculated for other conditions. The dip in the curve is due to the effect of expulsing high-concentration bitumen solution from the porous particles as the critical temperature is approached. After the drop, the rate increases due to the continued rise in temperature and then decreases as result of exhaustion of kerogen from the particles. The rate can be evaluated only from the predicted extraction curve since the experimental concentration is not known at reactor exit conditions.

Acknowledgment

The financial support of National Science Foundation, Grant No. CPE 83-11559, and Universidad Tecnica Federico Santa Maria is gratefully acknowledged.

Notation

A = absorbance of bitumen solution at 440 nm
a = absorptivity of bitumen solution, m^3/kg

a_m = external area of spherical particles per unit volume, m^{-1}
C_b = bitumen concentration in pores of particle, kg/m^3 solution
$C_{b,a}$ = concentration at spectrophotometer at $T = 298$ K, $P = 0.1$ MPa
$\underline{C}_{b,b}$ = bulk concentration in reactor
$\overline{C}_{b,b}$ = arithmetic average of concentrations of feed and effluent from differential reactor
$C_{b,e}$ = concentration in reactor effluent
C_k = kerogen concentration, kg/m^3 particle
C_p = heat capacity, kJ/kg · K
$C_{p_{os}}$ = value for raw shale
D = diffusivity of bitumen in toluene, m^2/s
D_c = diffusivity of bitumen at toluene critical point, m^2/s
D_e = effective diffusivity of bitumen in toluene in porous particles, m^2/s
d_p = particle diameter, m
E_a = activation energy, kJ/mol
$E(t)$ = age distribution function, Eq. 5, s
F = Fisher assay, m^3 oil/kg shale
h = particle-fluid heat transfer coefficient, kJ/m · s · K
k_o = preexponential factor, Eq. 9, s^{-1}
k_c = particle-fluid mass transfer coefficient, m/s
L = length of bed of particles, m
m = heating rate, K/s
m_o = initial mass of shale particles after dissolving initial bitumen, kg
N = number of points in summation, Eq. 31
P = pressure, MPa
P_c = critical pressure
$P_r = P/P_c$
Pr = Prandtl number of fluid, $C_p \mu/\lambda$
q = flow rate, m^3/s
Re = Reynolds number of fluid, $d_p u \rho/\mu$
R_g = gas constant, kJ/mol · K
R_o = particle radius, m
r = intraparticle radial position, m
$rmsd$ = root mean square deviation
Sc = Schmidt number of fluid, $\mu/\rho D$
T = temperature, K
T_b = bulk fluid temperature
T_c = critical temperature
$T_r = T/T_c$
t = time, s
u = superficial fluid velocity, m/s
V = volume of reactor bed, m
v_r = radial fluid velocity in pores, m/s
x = axial distance from entrance of bed, m

Greek letters

∂_m = mass of kerogen extracted, kg
ϵ_b = bed void fraction
ϵ_p = particle porosity
η_{os} = thermal diffusivity of oil shale, m^2/s
λ = fluid thermal conductivity, J/s · m · K
μ = fluid viscosity, Pa/s
ρ = fluid density, kg/m^3
ρ_a = density at spectrophotometer at $T = 298$ K, $P = 0.1$ MPa
ρ_b = density of bulk fluid
ρ_c = density at toluene critical point
ρ_e = density at reactor exit conditions
ρ_{os} = density of oil shale
$\rho_r = \rho/\rho_c$
Φ = objective function, Eq. 31
Ω = global reaction-extraction rate, Eq. 24, kg/s · kg

Literature Cited

Braun, R. L., and A. K. Burnham, "Kinetics of Colorado Oil Shale Pyrolysis in a Fluidized-Bed Reactor," *Fuel*, **65**, 218 (1986).

Chang, H. C., "Multiscale Analysis of Effective Transport in Periodic Heterogeneous Media," *Chem. Eng. Commun.*, **15**, 83 (1982).

Charlesworth, J. M., "Time and Temperature Dependence of Product Composition," *Ind. Eng. Chem. Process Des. Dev.*, **24**, 1117 (1985).

de Filippi, R. P., V. J. Krukonis, R. J. Robey, and M. Modell, "Supercritical Fluid Regeneration of Activated Carbon for Adsorption of Pesticides," EPA Rept. 600/2-80-0511 (Mar., 1980).

Golubev, I. F., "Viscosity of Gases and Gas Mixtures," *Nat. Tech. Inform. Serv.* **TT 70**, 50022 (1959).

Lee, B. I., and M. G. Kesler, "A Generalized Thermodynamic Correlation Based on Three-Parameter Corresponding States," *AIChE J.*, **21** 510 (1975).

Ludwig, R., L. A. Estevez, and J. M. Smith, "The Differential Reactor Approximation Under Dynamic Conditions," *Chem. Eng. Sci.*, **40**, 759 (1985).

McCarthy, H. E., G. Y. Cha, and W. J. Bartel, "Oil Shale and Tar Sands," *AIChE Symp. Ser.*, No. 155 (1976).

Pan, Z., H. Y. Feng, and J. M. Smith, "Rates of Pyrolysis of Colorado Oil Shale," *AIChE J.*, **31**, 721 (1985).

Paulaitis, M. E., V. J. Krukonis, R. T. Kurnik, and R. C. Reid, "Supercritical Fluid Extraction," *Rev. Chem. Eng.*, **1**, 179 (1983).

Reid, R. C., J. M. Prausnitz, and T. K. Sherwood, *The Properties of Gases and Liquids*, 3rd ed., McGraw-Hill, New York (1977).

Richardson, J. H., E. B. Huss, L. L. Ott, J. E. Clarkson, M. O. Bishop, J. R. Taylor, L. J. Gregory, and C. J. Morris, "Fluidized-Bed Pyrolysis of Oil Shale," Rept. UCID-19548, Lawrence Livermore Nat. Lab., Livermore, CA (1982).

Roy, D., and G. Thodos, "Thermal Conductivity of Gases, Organic Compounds at Atmospheric Pressure," *Ind. Eng. Chem.*, **9**, 71 (1970).

Stiel, L. I., and G. Thodos, "The Thermal Conductivity of Nonpolar Substances in the Dense Gaseous and Liquid Regions," *AIChE J.*, **10**, 26 (1964a).

———, "The Viscosity of Polar Substances in the Dense Gaseous and Liquid Regions," *AIChE J.*, **10**, 275 (1964b).

Sun, C. K., and H. Chen, "Tracer Diffusion of Aromatic Hydrocarbons in Liquid Cyclohexane up to Its Critical Temperature," *AIChE J.*, **31**, 1510 (1985a).

———, "Diffusion of Benzene, Toluene, Naphthalene, and Phenanthrene in Supercritical Dense 2.3-Dimethylbutane," *AIChE J.*, **31**, 1904 (1985b).

———, "Tracer Diffusion in Dense Ethanol: A Generalized Correlation for Nonpolar and Hydrogen-Bonded Solvents," *AIChE J.*, **32**, 1367 (1986).

Trewhella, M. J., I. J. F. Proplett, and A. Grint, "Structure of Green River Oil Shale Kerogen," *Fuel*, **65**, 541 (1986).

Triday, J., "Supercritical Extraction of Kerogen from Oil Shale," Ph.D. Thesis, Univ. California, Davis (Feb., 1987).

Wakao, N., and S. Kaguei, *Heat and Mass Transfer in Packed Beds*, Gordon and Breach, New York (1982).

Wallman, P. H., P. W. Tamm, and B. C. Spars, "Oil Shale, Tar Sands and Related Materials," *Symp. Ser.* #163, Am. Chem. Soc., Washington, DC (1981).

Yang, H. S., and H. Y. Sohn, "Mathematical Analysis of the Effect of Retorting Pressure on Oil Yield and Rate of Oil Generation from Oil Shale," *Ind. Eng. Chem. Process Dev.*, **24**, 274 (1985).

Yucelen, F., N. Wakao, and J. M. Smith, "Kerogen Decomposition at Sub-Pyrolysis Temperatures," *AIChE J.*, **32**, 607 (1986).

Manuscript received June 1, 1987, and revision received Oct. 26, 1987.